Available online at www.sciencedirect.com
ScienceDirect
Ceramics International 37 (2011) 3343–3349
CERAMICS INTERNATIONAL
www.elsevier.com/locate/ceramint

# Structural and magnetic properties of zinc ferrite incorporated in amorphous matrix

Petru Pascuta [a,*], Adrian Vladescu [b], Gheorghe Borodi [c], Eugen Culea [a], Romulus Tetean [b]

[a] Technical University of Cluj Napoca, Physics Department, 400114 Cluj Napoca, Romania
[b] Babes-Bolyai University, Faculty of Physics, 400084 Cluj Napoca, Romania
[c] National Institute for Research and Development for Isotopic and Molecular Technologies, 400293 Cluj Napoca, Romania

Received 22 January 2011; received in revised form 6 April 2011; accepted 25 May 2011
Available online 1 June 2011

**Abstract**

Glass ceramics in the $(Fe_2O_3)_x{\cdot}(B_2O_3)_{(60-x)}{\cdot}(ZnO)_{40}$ ($x = 17.5$ and 20 mol%) system were prepared by the melt-quench method and characterized using X-ray diffraction (XRD), scanning electron microscopy (SEM), Fourier transform infrared (FTIR) and magnetization measurements. The samples contain a unique magnetic crystalline phase, the zinc ferrite ($ZnFe_2O_4$), embedded in an amorphous matrix. The $ZnFe_2O_4$ crystals precipitate during cooling from melting temperature. From the XRD data, the average unit-cell parameter, crystallite size and the quantitative ratio of the crystallographic phases in the samples were evaluated. FTIR data revealed that the $BO_3$ and $BO_4$ are the main structural units of these glass ceramics network. FTIR spectra of these samples show features at characteristic vibration frequencies of $ZnFe_2O_4$. From the magnetization curves it was found that the nanoparticles exhibit ferromagnetic interactions combined with superparamagnetism with a blocking temperature, $T_B$, which is composition dependent. In all samples hysteresis is present below $T_B$. The coercive field is dependent on composition and magnetic field being around $0.05\mu_B$/f.u. for measurements performed in maximum 0.4 T. Finally, the magnetic behavior of iron in this system is discussed.


*Keywords:* C. Magnetic properties; D. Glass ceramics; Zinc ferrite; XRD; SEM; FTIR

## 1. Introduction

Spinel ferrites, $MFe_2O_4$ (M = Zn, Mn, Co, Ni, Mg) are currently intriguing materials due to their promising applications in a variety of fields such as ferrofluid, magnetic drug delivery and information storage, medical and bio-inspired technology [1–6]. Glass ceramics containing ferrimagnetic, ferromagnetic or superparamagnetic particles have potentially useful applications in different fields of electronic products [7,8]. Low melting glasses have been widely used for lowering the sintering temperature and optimizing coefficient thermal expansion in the field of electric devices such as multi layer ceramic capacitor, low temperature cofired ceramics, plasma display panels, cathode ray tube, and electric modules [9,10]. On the other hand iron ions have strong bearing on electrical, optical and magnetic properties of glasses. In general the presence of iron ions in glasses is considered to assemble together and form clusters which exhibit superparamagnetic behavior and below the freezing temperature, individual spins are frozen in random directions because of antiferromagnetic interaction between nearby ions [11,12]. It was shown that the magnetic properties of the zinc ferrite $ZnFe_2O_4$ are highly affected by their particle size [13]. From neutron diffraction data was reported for the first time that bulk $ZnFe_2O_4$ that crystallizes in the normal spinel structure which contains two different cation sites, 8 tetrahedral A sites and 16 octahedral B sites per f.u., order antiferromagnetically around 10 K [14]. Later, neutron diffraction studies at different temperatures have shown the existence of an antiferromagnetic short range order already around 100 K and the coexistence of long and short range order below 10 K [15]. More recently Schäfer et al. [16] have reported from powder neutron diffraction studies that the magnetic properties of $ZnFe_2O_4$ compounds are different if the samples are differently treated: (i) antiferromagnetic long range

* Corresponding author. Tel.: +40 264 401 262; fax: +40 264 595 355.
*E-mail address:* petru.pascuta@phys.utcluj.ro (P. Pascuta).

0272-8842/$36.00 
doi:10.1016/j.ceramint.2011.05.134

order below 10.5 K if the sample was annealed and slowly cooled; (ii) absence of any long range order for the sample annealed and quenched; (iii) onset of ferromagnetic ordering at 500 K for nanocrystalline material. In a normal spinel all $Zn^{2+}$ ions are on A sites and all $Fe^{3+}$ ions on B sites. In a fully inverse spinel half of the $Fe^{3+}$ ions fully occupy the A sites while the remaining half of $Fe^{3+}$ ions and $Zn^{2+}$ share the B sites. It is possible that mixtures between the two configurations could occur and these are characterized by the degree of inversion which depends strongly on the preparation procedures [17]. The magnetic coupling in $ZnFe_2O_4$ compound occurs via super exchange between the $Fe^{3+}$ ions. The A–B interaction is stronger as compared with A–A and B–B ones. The zinc ferrite nanoparticles may have non-zero inversion degrees which leads to different magnetic properties. These materials may show ferromagnetism or ferrimagnetism combined with superparamagnetism [13]. The growth of nanoparticles in an amorphous matrix prevents their coarsening, aggregation and interaction. It was reported that the inter particle interaction can have a strong influence on the magnetic properties of the samples [18].

The purpose of the present work was to investigate by XRD, SEM, FTIR and magnetic measurements the glass ceramics in the system $(Fe_2O_3)_x{\cdot}(B_2O_3)_{(60-x)}{\cdot}(ZnO)_{40}$ ($x = 17.5$ and 20 mol%) in order to obtain information concerning structural and magnetic properties of these glass ceramics.

## 2. Experimental

Glass ceramics in the $(Fe_2O_3)_x{\cdot}(B_2O_3)_{(60-x)}{\cdot}(ZnO)_{40}$ system, with $x = 17.5$ and 20 mol%, have been prepared by traditional melting method using $Fe_2O_3$, $B_2O_3$ and ZnO of high purity (99.9%) in suitable proportion. The mechanically homogenized mixtures were melted in sintered corundum crucibles at 1300 °C in an electric furnace in air atmosphere. The samples were put into the electric furnace directly at this temperature. After 30 min the molten material was quenched at room temperature by pouring onto a stainless-steel plate.

The XRD measurements were made with a XRD-6000 Shimadzu diffractometer, with a monochromator of graphite for the Cu-Kα radiation (λ = 1.54060 Å) at room temperature.

Microscopic examination of the samples was made with a Jeol JSM 5600-LV scanning electron microscope.

The FTIR absorption spectra of the glasses were obtained with a JASCO FTIR 6200 spectrometer in the 400–1600 $cm^{-1}$ spectral range with a resolution of 1 $cm^{-1}$. The IR absorption measurements were done using the KBr pellet technique. In order to obtain good quality spectra, the samples were crushed in an agate mortar to obtain particles of micrometer size. This procedure was applied every time to fragments of bulk glass to avoid structural modifications due to ambient moisture. At least two spectra for each sample were recorded. The spectra were normalized by making the absorption of any spectrum to vary from zero to one arbiter unit. Such normalization process was necessary to eliminate the concentration effect of the sample powder in the KBr disc.

Magnetic measurements were performed in the temperature range 4.2–300 K and external magnetic fields up to 12 T using the 12T Cryogen free vibrating sample magnetometer (VSM) equipment from Cryogenics. Direct current (DC) magnetization was recorded under zero-field cooled (ZFC) and field-cooled (FC) sequences under 0.05 and 0.1 T. Magnetic hysteresis loops were recorded at several temperatures below and above the blocking temperature.

## 3. Results and discussion

### 3.1. XRD and SEM data

The XRD patterns of the $(Fe_2O_3)_x{\cdot}(B_2O_3)_{(60-x)}{\cdot}(ZnO)_{40}$ ($x = 17.5$ and 20 mol%) glass ceramics are presented in Fig. 1. A characteristic amorphous halo can be observed in the $2\theta = 20–40^\circ$ range. The amorphous phase coexists with a crystalline phase since the diffraction pattern shows beside the large maxima overlapped with peaks characteristic to a crystalline phase. All detectable peaks can be indexed as belonging to the zinc ferrite crystalline phase, $ZnFe_2O_4$, in the standard data (PDF#221012). Zinc ferrite crystallizes in the face centered cubic system with Fd-3m space group. The lattice constant of zinc ferrite increases from $a = 8.33$ Å in the sample with $x = 17.5$ mol% to $a = 8.44$ Å in the sample with $x = 20$ mol%.

From the full width at half maximum for all peaks of the refined diffraction line profiles, the values of crystallite sizes of the crystalline phase were calculated by using the Debye–Scherrer formula given by [19]:

$$D = \frac{\lambda \cdot K}{\beta \cdot \cos\theta} \quad (1)$$

where $D$ is the apparent volume-weighted crystallite size, λ is the wavelength of X-rays (1.54060 Å, in this case), $K = 0.89$ (the Scherrer constant), $\theta$ is the angle of Bragg diffraction, $\beta = B - b$, $B$ is the full width, at half maximum and $b$ represents the instrumental line broadening. The crystal size of zinc ferrite

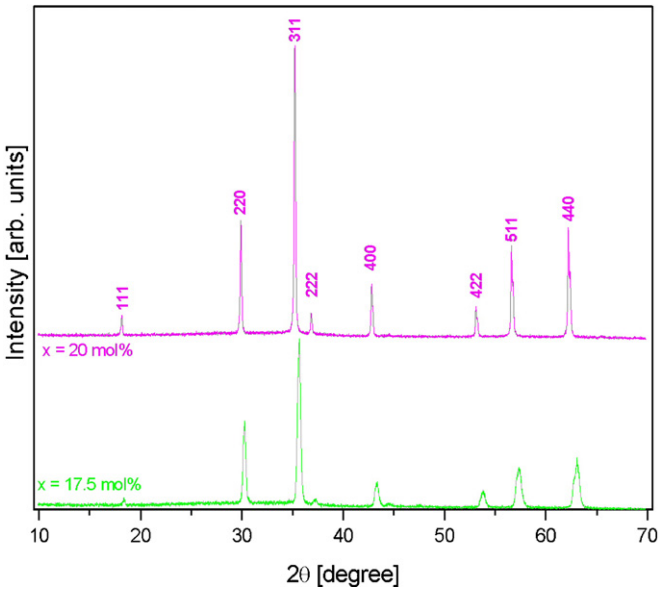


Fig. 1. The XRD patterns of $(Fe_2O_3)_x{\cdot}(B_2O_3)_{(60-x)}{\cdot}(ZnO)_{40}$ glass ceramics.

increases from 41 nm in the sample containing 17.5 mol% $Fe_2O_3$ to 98 nm in the sample with 20 mol% $Fe_2O_3$, so, the crystallite size grows with the amount of iron oxide. The degree of crystallinity was estimated using following relationship [20]:

$$X_c = \frac{I_c}{I_c + I_a} \times 100 \quad (2)$$

where $X_c$ is the crystallinity, $I_c$ is the integrated intensity of the crystalline phase which represents area of reflexion peaks, and $I_a$ is the integrated intensity of the amorphous phase, that is area of amorphous halo. The quantity of the crystallized phase is 68 wt% for the sample with 17.5 mol% $Fe_2O_3$ and 74 wt% for the sample with 20 mol%.

A large number of particles may be observed in the SEM micrographs of the studied samples – Fig. 2a and b. One can see that in the case of the $x = 17.5$ mol% sample the particles are well defined while in the case of the sample with $x = 20$ mol% an agglomeration of the particles and, in the same time, a texture is present. Sample containing 20 mol% $Fe_2O_3$ exhibits dendrites dispersed within the glass matrix. The distribution of the dendrites is homogeneous. Primary dendritic axes have a length of 20–30 μm, and primary dendrites show some evidence of texturing as expected, since the dendrites tend to grow along the direction of the local temperature gradient. The particles observed by SEM in these samples have a size larger than that calculated by the Scherrer method. This may be explained by the thermodynamic conditions at the surface of the samples which propitiate the growth of crystals. The majority of zinc ferrite crystals contributing to the XRD patterns are located inside the samples and therefore with average particle sizes much smaller than those observed at their surface.

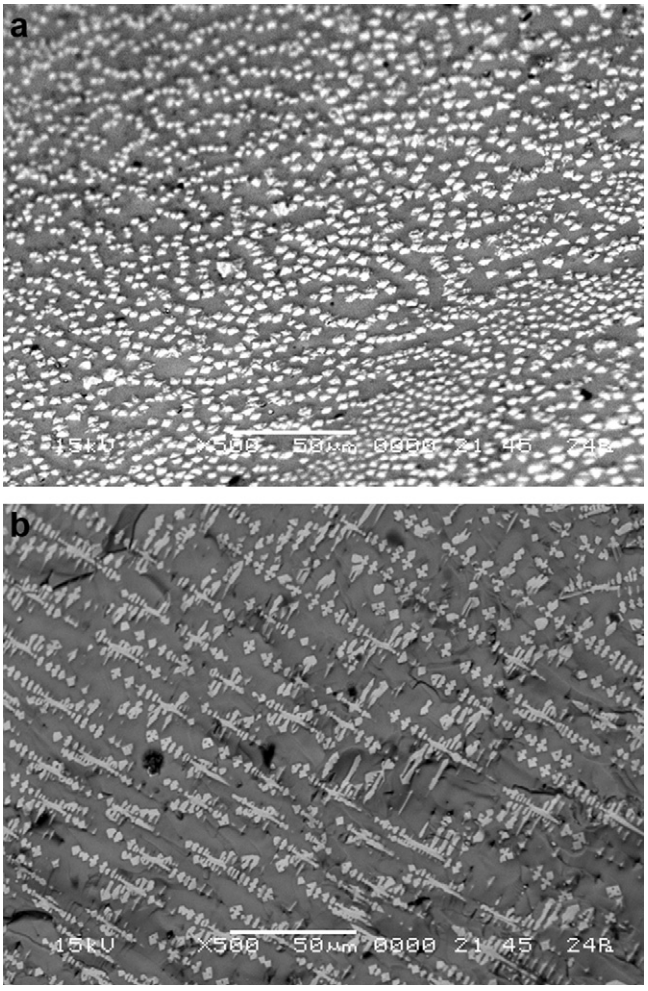


Fig. 2. SEM micrographs of the samples with $x = 17.5$ mol% (a) and $x = 20$ mol% (b).

### 3.2. FTIR data

Fig. 3 shows the FTIR spectra of the $(Fe_2O_3)_x \cdot (B_2O_3)_{(60-x)} \cdot (ZnO)_{40}$ ($x = 17.5$ and 20 mol%) glass ceramics. To get quantitative information about the structural groups in the studied samples, the FTIR spectra have been deconvoluted. This procedure was made using the Spectra Manager program and a Gaussian type function. The use of the deconvolution procedure allowed us a better identification of the absorption bands which appear in these spectra and their more precise assignment. Fig. 4 shows the deconvolution, in Gaussian bands, of the spectrum for the sample containing 20 mol% $Fe_2O_3$. The deconvolution parameters, the band centers $C$ and the relative area $A$ as well as the band assignment are given in Table 1 for the studied samples. The peak from 421–464 $cm^{-1}$ is attributed to the vibration of the chemical bond ($Fe^{3+}$–$O^{2-}$) in B location of the octahedron and the band from 560–587 $cm^{-1}$ is attributed to the vibration of the chemical bond ($Zn^{2+}$–$O^{2-}$) in A location of the tetrahedron, respectively [21,22]. These bands confirm the presence of zinc ferrite in the studied samples. The intensity of these bands increases with the increasing of iron ions content. FTIR spectrum of studied samples contains all the important bands of vitreous $B_2O_3$, but shifted from their original position. So, in all IR spectra there is an intense band located at 681–691 $cm^{-1}$ corresponding to the band at 720 $cm^{-1}$ from the vitreous IR spectrum of $B_2O_3$, attributed to B–O–B bending vibrations

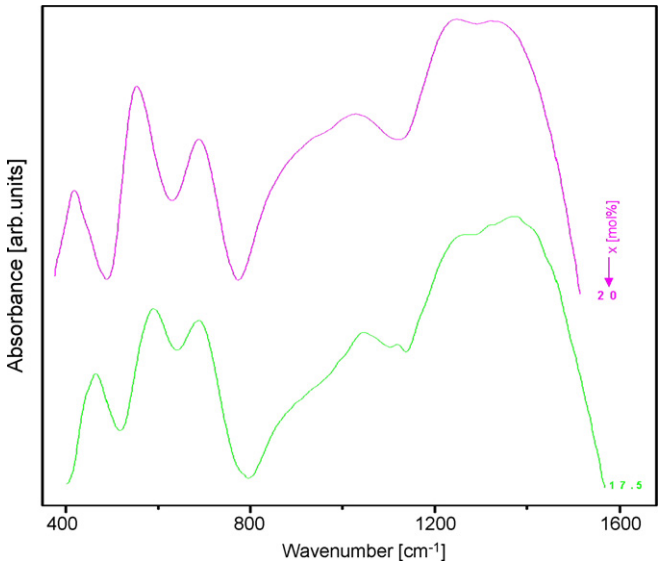


Fig. 3. FTIR spectra of the $(Fe_2O_3)_x \cdot (B_2O_3)_{(60-x)} \cdot (ZnO)_{40}$ glass ceramics.

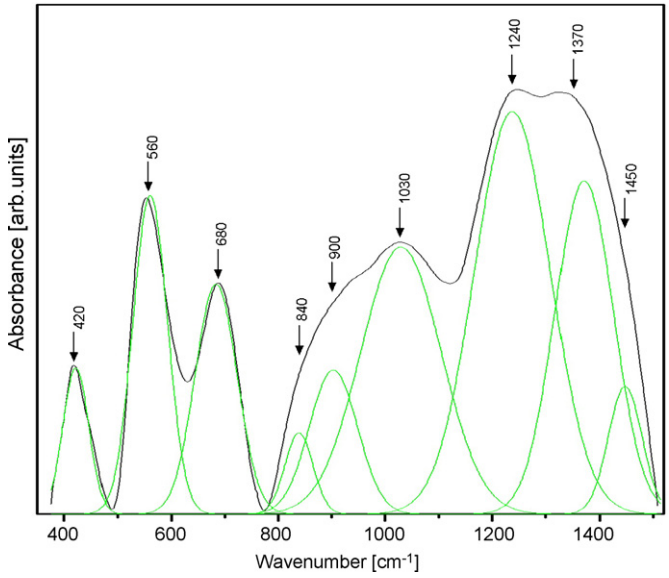


Fig. 4. Deconvoluted FTIR spectra of the samples with $x = 20$ mol% glass ceramic using a Gaussian-type function.

[23–27]. The peaks from 838–857 $cm^{-1}$ and 1029–1042 $cm^{-1}$ are due to the stretching vibrations of B–O bonds in $BO_4$ units from tri-, tetra- and penta-borate groups while the peak from 902–920 $cm^{-1}$ can be attributed to the stretching vibrations of B–O bonds in $BO_4$ units from diborate groups [23–27]. The absorption band from 1237–1247 $cm^{-1}$ is attributed to the stretching vibrations of B–O bonds in $BO_3$ units from boroxol rings. The absorption band from 1371–1394 $cm^{-1}$ can be due to the stretching vibrations of B–O in $BO_3$ units from different borate groups. Finally, the band located at 1447–1482 $cm^{-1}$ is attributed to the stretching vibrations of $B–O^-$ in $BO_2O^-$ units from different borate groups [23–27]. To quantify the iron ions effect to the changes in the relative population of threefold and fourfold boron atoms we have calculated the fraction of four-coordination boron atoms, $N_4$, as was defined previously [28–30]:

$$N_4 = \frac{A_4}{A_3 + A_4} \quad (3)$$

where $A_4$ and $A_3$ denote the areas of $BO_4$ units (the areas of component bands from 838–857 $cm^{-1}$, 902–920 $cm^{-1}$ and 1029–1042 $cm^{-1}$) and $BO_3$ units (the areas of component bands from 1237–1245 $cm^{-1}$, 1371 –1394 $cm^{-1}$ and 1447–1482 $cm^{-1}$), respectively. The fraction of four-coordination boron atoms, $N_4$, increases with increasing the content of $Fe_2O_3$ from 0.25 for $x = 17.5$ mol% to 0.36 for $x = 20$ mol%. This is due to the structural changes involving the conversions of the $BO_3$ into $BO_4$ structural units as the content of the $Fe_2O_3$ increases. The $BO_3 \rightarrow BO_4$ conversion process increases the stability of the studied samples. The threefold boron atoms are favored in the investigated system as compared with the fourfold ones.

### 3.3. Magnetic data

The DC-magnetization data taken as ZFC/FC curves for applied magnetic fields of 0.05 and 0.1 T are presented in Fig. 5. The ZFC magnetization curves show well defined broad peaks that are centered at approximately 34 K ($x = 17.5$ mol%), respectively 37 K ($x = 20$ mol%). Below these temperatures irreversible behavior sets in. These broad peaks coincide with the bifurcation temperature of the ZFC–FC magnetization and could be associated with the superparamagnetic blocking temperature of the nanoparticles, $T_B$ [31]. This behavior can be explained by the progressive magnetic blocking of magnetic nanoparticles whose size determines a magnetic anisotropy comparable to the thermal energy [32]. One can see that the bifurcation point between the FC and ZFC curves shifts to lower temperatures as the magnetic field used for the measurements increases, which is another sign of the superparamagnetic behavior [17,33,34]. The FC magnetization curve, for the temperatures below the bifurcation point, continues to rise. This behavior is characteristic of a superparamagnetic system [33] while in spin glass materials the magnetization is almost flat. Magnetization isotherms measured at 5 K in magnetic fields up to 12 T are presented in Fig. 6. One can see that no saturation is attended. The iron magnetic moment at 5 K in 12 T external magnetic field is $2.3\mu_B$/Fe atom for the sample with $x = 20$ mol% and $1.66\mu_B$/Fe atom for $x = 17.5$ mol%. The increase on iron magnetic moment with iron concentration could be explained by the increase of the magnetic coupling in $ZnFe_2O_4$ which occurs via super exchange between the $Fe^{3+}$ ions. In a normal spinel all $Zn^{2+}$ ions are on A sites and all $Fe^{3+}$ ions on B sites while in a fully

Table 1
Deconvolution parameters (the band centers $C$ and the relative areas $A$) and the band assignments for the $(Fe_2O_3)_x{\cdot}(B_2O_3)_{(60-x)}{\cdot}(ZnO)_{40}$ glass ceramics.

| $x = 17.5$ | | $x = 20$ | | Assignments |
|---|---|---|---|---|
| $C$ | $A$ | $C$ | $A$ | |
| 464 | 26.3 | 421 | 20.8 | $Fe^{3+}$–$O^{2-}$ vibration in B location of the octahedron |
| 587 | 62.9 | 560 | 60.7 | $Zn^{2+}$–$O^{2-}$ vibration in A location of the tetrahedron |
| 691 | 54.7 | 683 | 53.2 | B–O–B bend |
| 857 | 7.5 | 838 | 12.5 | B–O stretch in $BO_4$ units from tri-, tetra- and penta-borate groups |
| 920 | 26.2 | 902 | 38.3 | B–O stretch in $BO_4$ units from di-borate groups |
| 1042 | 81.5 | 1029 | 118.8 | B–O stretch in $BO_4$ units from tri-, tetra- and penta-borate groups |
| 1245 | 171 | 1237 | 167.8 | B–O stretch in $BO_3$ units from boroxol rings |
| 1394 | 127.8 | 1371 | 107.2 | B–O stretch in $BO_3$ units from varied types of borate groups |
| 1482 | 32.9 | 1447 | 23.7 | $B–O^-$ stretch in $BO_2O^-$ units from varied types of borate groups |

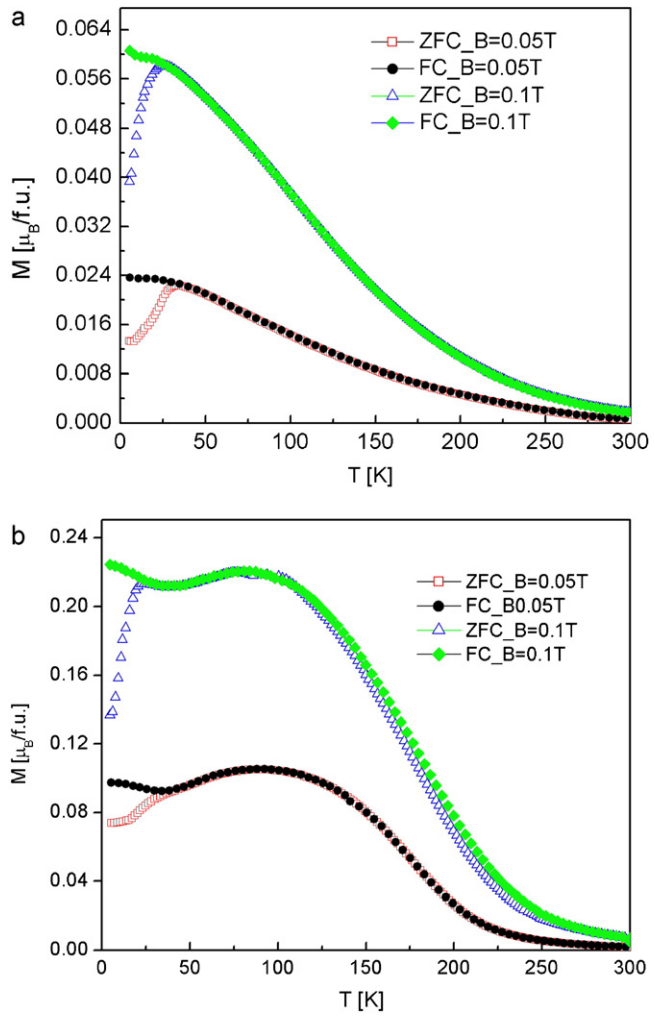


Fig. 5. The temperature dependence of the magnetization in zero field cooled (ZFC) and field cooled (FC) measured in 0.05 and 0.1 T for the sample with $x = 17.5$ mol% (a) and $x = 20$ mol% (b).

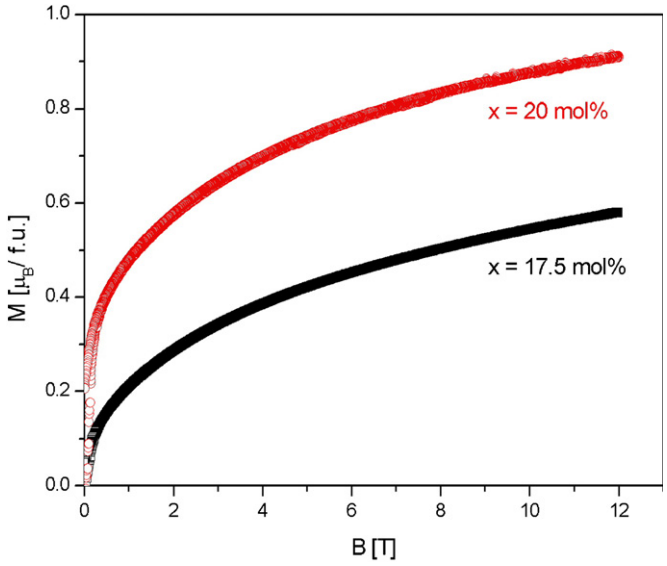


Fig. 6. Magnetization isotherms at 5 K in external fields up to 12 T $(Fe_2O_3)_x{\cdot}(B_2O_3)_{(60-x)}{\cdot}(ZnO)_{40}$ glass ceramics.

inverse spinel half of the $Fe^{3+}$ ions fully occupy the A sites while the remaining half of $Fe^{3+}$ ions and $Zn^{2+}$ share the B sites. Probably, in our samples, mixtures between the two configurations occur and these are characterized by the degree of inversion [17]. In our sample the degree of inversion could increase with the increase of iron concentration and more $Fe^{3+}$ ions occupy the B sites. The A–B interaction is stronger as compared with A–A and B–B ones and as a consequence the iron magnetic moment increase. On the other hand the inter particle interaction can have a strong influence on the magnetic properties of the samples [18]. In the sample with $x = 20$ mol% the average size of the zinc ferrite is higher and a texture was revealed by SEM micrographs. The average distances between particles are lower in this sample and the magnetic interaction is stronger. These could be a reason too for the increase of iron magnetic moment. The external magnetic field dependence of the magnetization at various temperatures above and below $T_B$ for the sample with $x = 17.5$ mol% is shown in Fig. 7. Similar behavior was obtained for the sample with $x = 20$ mol%. Because of the nanoparticle's magnetic anisotropy, the magnetic moment is always in one of two energy minima, separated by an energy barrier. At finite temperature, there is a finite probability for the magnetization to flip and reverse its direction. The mean time between two flips is called the Néel relaxation time and is given by the following Néel–Arrhenius equation [35]:

$$\tau = \tau_0 \cdot \exp\left(\frac{E_B}{k_B T}\right) \tag{4}$$

where $\tau_0$ is a constant and $E_B$ is energy barrier. One can see that the relaxation time increases with decreasing temperature. For all the samples hysteresis is present even at temperatures higher than $T_B$. For example, the coercitive field decreases with increasing temperature from 0.07 T at 5 K to 0.02 T at 50 K for the sample with $x = 20$ mol%. Hysteresis is present at higher temperatures contrary as expected for a system of non-interacting superparamagnetic particles [34]. The observed loops are identical and symmetric about their center which is char-

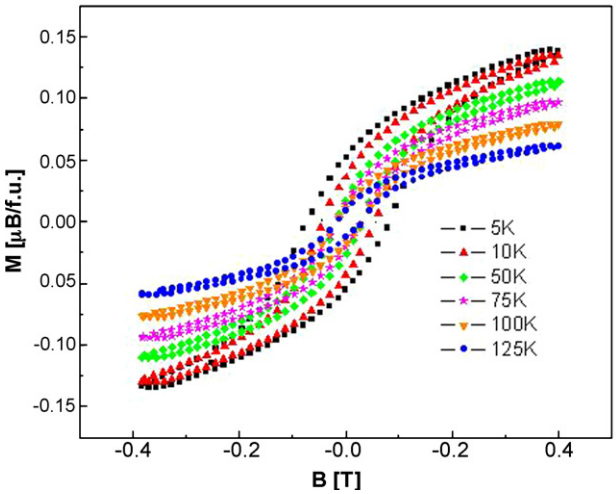


Fig. 7. Magnetization hysteresis loops for the sample with $x = 17.5$ mol% at different temperatures.

acteristic of superparamagnetic behavior [17,36,37]. This behavior is characteristic of both superparamagnetic and spin glass systems [38]. The presence of hysteresis above $T_B$ can be explained by the presence of weak magnetic interactions between particles at these temperatures. Probably the energy barrier is still present above $T_B$ but is not high enough to stop the magnetic moment oscillations during the measuring time.

## 4. Conclusions

In this study glass ceramics containing a unique magnetic crystalline phase (zinc ferrite crystals) embedded in an amorphous matrix were synthesized. These glass ceramics contain 68 wt% zinc ferrite for the sample with $x = 17.5$ mol% and 74 wt% zinc ferrite for the sample with $x = 20$ mol%. The crystalline phase is produced during the cooling from the melting temperature to room temperature. No other subsequent nucleation and crystallization treatments are necessary.

The FTIR studies show that the glass ceramic network consists of $BO_3$ and $BO_4$ units, but their proportion depends on the iron ion content in the samples. The increase of iron ion content in the investigated samples increases their stability. The FTIR spectra, namely the absorption bands from 421–464 $cm^{-1}$ and from 560–587 $cm^{-1}$ confirm the presence of $ZnFe_2O_4$.

From the magnetic measurements we conclude that characteristics of both superparamagnetic and spin glass systems are present. Thus, the blocking temperature that shifts to lower temperatures as the magnetic field used for the measurements increases, the FC magnetization curve that, below the bifurcation point, continues to rise and the fact that no saturation is attended constitute characteristic of a superparamagnetic system. The magnetic loops are identical and symmetric about their center which is also characteristic of superparamagnetic behavior. Hysteresis is present at higher temperatures contrary as expected for a system of non-interacting superparamagnetic particles. In conclusion, the observed magnetic behavior is complex and further investigations are necessary in order to elucidate the properties of the studied materials.

## Acknowledgements

This work was supported by CNCSIS – UEFISCSU, project number PNII–IDEI 226/2008. A.V. wish to thank for the financial support provided from programs co-financed by The Sectoral Operational Programme Human Resources Development, Contract POSDRU 6/1.5/S/3 – ''Doctoral studies: through science towards society''.

## References

[1] P.P. Hankare, U.B. Sankpal, R.P. Patil, I.S. Mulla, R. Sasikala, A.K. Tripathi, K.M. Garadkar, Synthesis and characterization of nanocrystalline zinc substituted nickel ferrites, J. Alloys Compd. 496 (2010) 256–260.
[2] Y.-P. Fu, S.-H. Hu, Electrical and magnetic properties of magnesium-substituted lithium ferrite, Ceram. Int. 36 (2010) 1311–1317.
[3] N. Sivakumar, A. Narayanasamy, J.-M. Greneche, R. Murugaraj, Y.S. Lee, Electrical and magnetic behaviour of nanostructured $MgFe_2O_4$ spinel ferrite, J. Alloys Compd. 504 (2010) 395–402.
[4] S.F. Mansour, M.A. Elkestawy, A comparative study of electric properties of nano-structured and bulk Mn Mg spinel ferrite, Ceram. Int. 37 (2010) 1175–1180.
[5] J.E. Tasca, C.E. Quincoces, A. Lavat, A.M. Alvarez, M.G. Gonzalez, Preparation and characterization of $CuFe_2O_4$ bulk catalysts, Ceram. Int. 37 (2010) 803–812.
[6] M.A. Hakim, M. ManjurulHaque, M. Huq, P. Nordblad, Spin-glass-like ordering in the spinel $ZnFe_2O_4$ ferrite, Physica B 406 (2011) 48–51.
[7] H.-I. Hsiang, T.-H. Chen, Electrical properties of low-temperature-fired ferrite–dielectric composites, Ceram. Int. 35 (2009) 2035–2203.
[8] R.K. Singh, A. Srinivasan, Bioactivity of ferrimagnetic MgO–CaO–$SiO_2$–$P_2O_5$–$Fe_2O_3$ glass-ceramics, Ceram. Int. 36 (2010) 283–290.
[9] L. Zhou, H. Lin, W. Chen, L. Lua, IR and Raman investigation on the structure of $(100 - x)B_2O_3 - x$[0.5 BaO–0.5 ZnO] glasses, J. Phys. Chem. Solids 69 (2008) 2499–2502.
[10] K.S. Kim, S.H. Shim, S. Kim, S. Ok Yoon, Low temperature and microwave dielectric properties of $TiO_2$/ZBS glass composites, Ceram. Int. 36 (2010) 1571–1575.
[11] S.M. Del Nery, W.M. Pontuschka, S. Isotani, C.G. Rouse, Luminescence quenching by iron in barium aluminoborate glasses, Phys. Rev. B 49 (1994) 3760–3765.
[12] G. Srinivasarao, N. Veeraiah, The role of iron ions on the structure and certain physical properties of PbO–$As_2O_3$ glasses, J. Phys. Chem. Solids 63 (2002) 705–717.
[13] F.J. Burghart, W. Potzel, G.M. Kalvius, E. Schreier, G. Grosse, D.R. Noakes, W. Schafer, W. Kockelmann, S.J. Campbell, W.A. Kaczmarek, A. Martin, M.K. Krause, Magnetism of crystalline and nanostructured $ZnFe_2O_4$, Physica B 289–290 (2000) 286–290.
[14] J.M. Hasting, L.M. Corliss, An antiferromagnetic transition in zinc ferrite, Phys. Rev. 102 (1956) 1460–1463.
[15] Y.G. Chukalkin, V.R. Shtirts, Characteristics of the magnetic state of $ZnFe_2O_4$, Sov. Phys. Solid State 30 (1988) 1683–1686.
[16] W. Schäfer, W. Kockelmann, A. Kirfel, W. Potzel, F.J. Burghart, G.M. Kalvius, A. Martin, W.A. Kaczmarek, S.J. Campbell, Structural and magnetic variations of $ZnFe_2O_4$ spinels-neutron powder diffraction studies, Mater. Sci. Forum 321–324 (2000) 802–807.
[17] M.G. Ferreira da Silva, L.C.J. Pereira, J.C. Waerenborgh, Precipitation of zinc ferrite nanoparticles in the $Fe_2O_3$–ZnO–$SiO_2$ glass system, J. Non-Cryst. Solids 353 (2007) 2374–2382.
[18] S. Mřrup, C. Frandsen, F. Bodker, S.N. Klausen, K. Lefmann, P. Lindgard, M.F. Hansen, Magnetic properties of nanoparticles of antiferromagnetic materials, Hyperfine Interact. 144–145 (2002) 347–357.
[19] H. Klug, L. Alexander, X-ray Diffraction Procedures for Polycrystalline and Amorphous Materials, John Wiley & Sons, Inc., London, 1962.
[20] P. Pascuta, G. Borodi, N. Jumate, I. Vida-Simiti, D. Viorel, E. Culea, The structural role of manganese ions in some zinc phosphate glasses and glass ceramics, J. Alloys Compd. 504 (2010) 479–483.
[21] G.Q. Yang, B. Han, Z.T. Sun, L.M. Yan, S.Y. Wang, Preparation and characterization of brown nanometer pigment with spinel structure, Dyes Pigments 55 (2002) 9–16.
[22] Y. Koseoglu, A. Baykal, M.S. Toprak, F. Gozuak, A.C. Basaran, B. Aktas, Synthesis and characterization of $ZnFe_2O_4$ magnetic nanoparticles via a PEG-assisted route, J. Alloys Compd. 462 (2008) 209–213.
[23] M. Abo-Naf, F.H.El Batal, M.A. Azooz, Characterization of some glasses in the system $SiO_2$, $Na_2O$·RO by infrared spectroscopy, Mater. Chem. Phys. 77 (2002) 846–852.
[24] A. Kumar, S.B. Rai, D.K. Rai, Effect of thermal neutron irradiation on $Gd^{3+}$ ions doped in oxyfluoroborate glass: an infra-red study, Mater. Res. Bull. 38 (2003) 333–339.
[25] I. Ardelean, P. Pascuta, Comparative vibrational study of $xFe_2O_3·(1 - x)$[$3B_2O_3$·MO] (MO ⇒ CaO or $CaF_2$) glass systems, Mater. Lett. 58 (2004) 3499–3502.
[26] P. Pascuta, G. Borodi, E. Culea, Influence of europium ions on structure and crystallization properties of bismuth borate glasses and glass ceramics, J. Non-Cryst. Solids 354 (2008) 5475–5479.

[27] P. Pascuta, Structural investigations of some bismuth–borate–vanadate glasses doped with gadolinium ions, J. Mater. Sci.: Mater. Electron. 21 (2010) 338–342.
[28] K. El-Egili, Infrared studies of $Na_2O$–$B_2O_3$–$SiO_2$ and $Al_2O_3$–$Na_2O$–$B_2O_3$–$SiO_2$ glasses, Physica B 325 (2003) 340–348.
[29] P. Pascuta, L. Pop, S. Rada, M. Bosca, E. Culea, The local structure of bismuth borate glasses doped with europium ions evidenced by FT-IR spectroscopy, J. Mater. Sci.: Mater. Electron. 19 (2008) 424–428.
[30] P. Pascuta, G. Borodi, E. Culea, Structural investigation of bismuth borate glass ceramics containing gadolinium ions by X-ray diffraction and FTIR spectroscopy, J. Mater. Sci.: Mater. Electron. 20 (2009) 360–365.
[31] Y. Ichiyanagi, Y. Moro, H. Katayanagi, S. Kimura, D. Shigeoka, T. Hiroki, T. Mashino, Magnetic and thermal analysis of $MFe_2O_4$ (M = Co, Mn, Zn) nanoparticles, J. Therm. Anal. Calorim. 99 (2010) 83–86.
[32] C. Cannas, D. Gatteschi, A. Musinu, G. Piccaluga, C. Sangregorio, Structural and magnetic properties of $Fe_2O_3$ nanoparticles dispersed over a silica matrix, J. Phys. Chem. B 102 (1998) 7721–7726.
[33] J.K. Vassiliou, V. Mehrotra, M.W. Russell, R.D. McMicael, R.D. Schull, R.F. Ziolo, Magnetic and optical properties of γ-$Fe_2O_3$ nanocrystals, J. Appl. Phys. 73 (1993) 5109–5116.
[34] G.F. Goya, E.R. Leite, Ferrimagnetism and spin canting of Zn $^{57}$ $Fe_2O_4$ nanoparticles embedded in ZnO matrix, J. Phys.: Condens. Matter 15 (2003) 641–652.
[35] L. Néel, Théorie du traînage magnétique des ferromagnétiques en grains fins avec applications aux terres cuites, Ann. Géophys. 5 (1949) 99–136.
[36] A. Mydosh, Spin Glasses: An Experimental Introduction, Taylor and Francis, London, 1993.
[37] J.L. Garcıa, A. Lopez, F.J. Lazaro, C. Martınez, A. Corma, Iron oxide particles in large pore zeolites, J. Magn. Magn. Mater. 157–158 (1996) 272–273.
[38] M.D. Mukadam, S.M. Yusuf, P. Sharma, S.K. Kulshreshtha, Magnetic behavior of field induced spin-clusters in amorphous $Fe_2O_3$, J. Magn. Magn. Mater. 269 (2004) 317–326.